PROCEEDINGS OF SCIENCE

Low-energy $e^+e^- \to hadrons$ cross sections and $g-2$ of the muon

J. William Gary*
Department of Physics and Astronomy, University of California, Riverside, CA 92521, USA
E-mail: bill.gary@ucr.edu

Results on low-energy $e^+e^- \to hadrons$ cross sections are presented, and the relationship to the anomalous magnetic moment of the muon is explained. Recent results from Babar emphasizing low-energy hadronic cross sections with kaons in the final state are presented, based on the initial-state photon radiation method to obtain small effective hadronic center-of-mass energies.

Flavor Physics & CP Violation 2015,
May 25-29, 2015
Nagoya, Japan

*Speaker.

PoS(FPCP2015)045

1. Introduction

The gyromagnetic ratio g specifies the relationship between an angular momentum and the corresponding magnetic moment. The Dirac result for the gyromagnetic ratio g_ℓ of an elementary charged spin-1/2 lepton ℓ is $g_\ell = 2$ exactly. The Dirac result corresponds to the tree level diagram shown in the leftmost plot of Fig. 1. Radiative corrections alter the prediction to $g_\ell = 2(1 + a_\ell)$, introducing sensitivity to new physics through loops. The term a_ℓ is known as the anomalous moment, expressed as $a_\ell = (g_\ell - 2)/2$ and simplified in common parlance to "$g-2$". The muon anomaly a_μ is much more sensitive to virtual heavy particle production in loops than the electron anomaly a_e because the relative virtual terms scale like $(m_\mu/m_e)^2 \approx 43{,}000$, with m_ℓ the lepton mass.

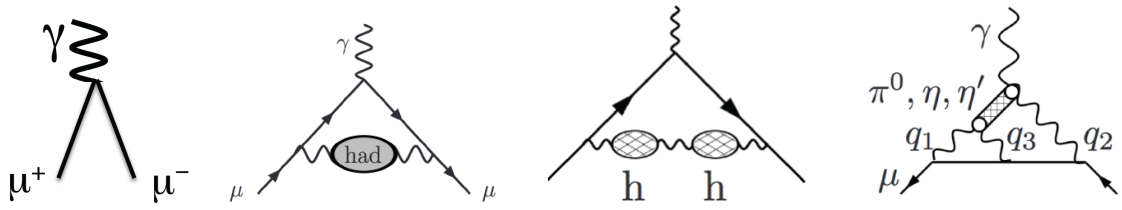

Figure 1: (left) Tree-level vertex diagram for a muon coupling to a photon and (left-center) the diagram corresponding to the leading-order hadronic correction. Examples of diagrams for the higher-order hadronic corrections and for light-by-light scattering are shown in the right-center and right plots, respectively. The three leftmost plots are taken from Ref. [1].

In the standard model (SM), $a_\mu = a_\mu^{QED} + a_\mu^{EW} + a_\mu^{had}$, receiving contributions from electromagnetic, weak, and hadronic loop corrections. The purely electromagnetic term a_μ^{QED} has been calculated [2] to tenth order in the fine structure constant α. The electroweak term a_μ^{EW} [3] includes contributions from the recently discovered Higgs boson. The hadronic term a_μ^{had} is considered in three parts, illustrated by the three rightmost plots of Fig. 1: the leading-order hadronic vacuum polarization term $a_\mu^{had,LO-VP}$, the higher-order hadronic vacuum polarization terms $a_\mu^{had,HO-VP}$, and the so-called light-by-light scattering term $a_\mu^{had,LbLs}$. A summary of the individual contributions to the SM result for a_μ is given in Table 1. Summing these contributions yields a total SM prediction of $a_\mu^{SM} = 1\,165\,91\,802 \pm 49 \times 10^{-11}$ [4], which lies $287 \pm 80 \times 10^{-11}$ below the average measured result, $a_\mu^{data} = 1\,165\,92\,091 \pm 63 \times 10^{-11}$ [5, 6], corresponding to a discrepancy of about 3.5 standard deviations. From Table 1 it is seen that the uncertainty in the SM prediction is dominated by the uncertainty in the leading-order vacuum polarization term $a_\mu^{had,LO-VP}$. This term will be the focus of the subsequent discussion.

The energy scale is too low for $a_\mu^{had,LO-VP}$ to be calculated perturbatively, and lattice calculations [7] are not yet sufficiently precise. Instead, the most precise result for $a_\mu^{had,LO-VP}$ is obtained from low-energy $e^+e^- \to hadrons$ data, using the optical theorem and the following dispersion integral (see Ref. [6]):

$$a_\mu^{had,LO-VP} = \left(\frac{\alpha}{3\pi}\right)^2 \int_{m_\pi^2}^{\infty} \frac{K(s) R_{had}}{s} ds, \tag{1.1}$$

where $K(s)$ is a kinematic factor and R_{had} is the $e^+e^- \to hadrons$ cross section normalized to the $e^+e^- \to \mu^+\mu^-$ cross section. Because of the $1/s$ factor, low-energy contributions dominate the

Table 1: SM results for the different contributions to the muon anomaly a_μ, taken from Ref. [4].

a_μ term	SM prediction ($\times 10^{-11}$)
a_μ^{QED}	116584718.951 ± 0.080
a_μ^{EW}	153.6 ± 1.0
$a_\mu^{had,LO-VP}$	6923 ± 42
$a_\mu^{had,HO-VP}$	-98.4 ± 0.7
$a_\mu^{had,LbLs}$	105 ± 26

dispersion integral. Therefore precise measurements of R_{had} are needed at low values of center-of-mass energy $\sqrt{s}$. Below $\sqrt{s} = 2$ GeV, the sum of exclusive hadronic channels is used because the background from $e^+e^- \to e^+e^-$ and $e^+e^- \to \mu^+\mu^-$ events is difficult to distinguish from inclusive multihadronic events at such low energies. Also, the inclusive detection efficiency is difficult to measure with precision at very low $\sqrt{s}$. For energies above 2 GeV, inclusive $e^+e^- \to$ *hadrons* data and perturbative calculations can be used.

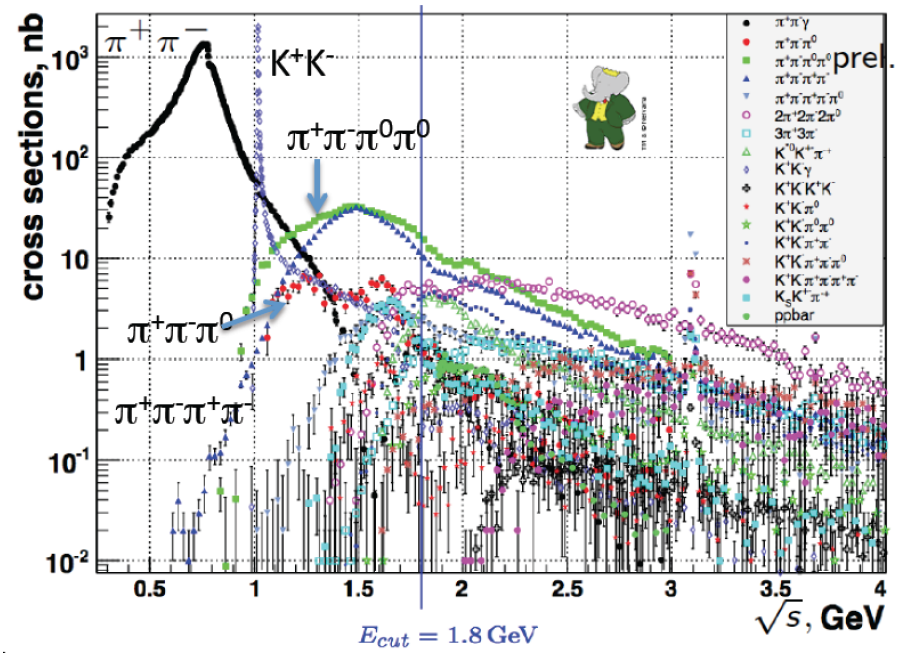

Figure 2: Summary of Babar measurements of low-energy exclusive hadronic cross sections.

Figure 2 shows measurements of exclusive hadronic cross sections from the Babar Collaboration. Some of these results are discussed below. These results establish that the $e^+e^- \to \pi^+\pi^-$ channel dominates the low-energy hadronic cross section. It contributes about 75% of the area to the dispersion integral. The 3π and 4π channels are also important, as are channels with kaons for energies above the ϕ meson mass. Table 2 lists the channels whose uncertainties in the cross section contribute the most to the uncertainty $\Delta a_\mu^{had,LO-VP}$ in $a_\mu^{had,LO-VP}$. The largest contribution to $\Delta a_\mu^{had,LO-VP}$ comes from the $\pi^+\pi^-$ channel, followed by the $\pi^+\pi^-\pi^0$ and $\pi^+\pi^-\pi^0\pi^0$ channels. Reducing the uncertainties in dikaon channels are also seen to be important.

In the following, improved measurements for all the channels listed in Table 2 are discussed, with the exception of the two four-pion channels. The data are collected either through an energy scan (the CMD3, SND, and CLEO experiments), or with the initial-state radiation (ISR) method (the Babar, KLOE, and BESIII experiments). In the ISR method, an effective reduced hadronic energy $\sqrt{s'}$ is obtained by selecting events with a hard ISR photon radiated from either the incoming electron or incoming positron in fixed-energy e^+e^- collisions.

Table 2: Exclusive $e^+e^- \to$ *hadrons* channels contributing the largest uncertainty $\Delta a_\mu^{had,LO-VP}$ to the SM prediction of the muon anomaly term $a_\mu^{had,LO-VP}$ (taken from Ref. [4]).

Channel	$\pi^+\pi^-$	$\pi^+\pi^-\pi^0$	$\pi^+\pi^-\pi^0\pi^0$	K^+K^-	$\pi^+\pi^-\pi^+\pi^-$	$KK\pi\pi$	K_SK_L
$\Delta a_\mu^{had,LO-VP}$ $(\times 10^{-11})$	28	15	12	7	5	4	4

2. $e^+e^- \to \pi^+\pi^-(\pi^0)$ results from BESIII and VEPP-2000

Concerning the all-important $\pi^+\pi^-$ channel, the most precise published measurements are from the Babar [8] and KLOE [9, 10] experiments. Unfortunately, the results from the two experiments differ by more than the quoted uncertainties for energies above the ρ meson mass (see Ref. [8] for a discussion). New precise data are required to resolve this discrepancy and to reduce the uncertainty of the $e^+e^- \to \pi^+\pi^-$ cross section measurements.

New precise data from the BESIII experiment at the BEPC-II accelerator are now becoming available. Figure 3 (top left) shows preliminary measurements of the $e^+e^- \to \pi^+\pi^-$ cross section from BESIII, performed in the energy range from 0.6 to 0.9 GeV. Comparisons with Babar and KLOE are shown in Fig. 3 (top right) and (bottom), respectively. The comparisons are made by performing a fit to the BESIII data, and then dividing the results of Babar or KLOE by the results from the fit. The BESIII data are seen to lie slightly below the Babar data above the ρ meson mass but to lie around 1 standard deviation above the KLOE results for all energy values. The BESIII data are thus in better agreement with Babar than with KLOE. Nonetheless, the BESIII uncertainties are still fairly large and the BESIII data are not inconsistent with KLOE. The BESIII plan is to publish these data with reduced uncertainties once the luminosity determination is improved. Measurements of the $e^+e^- \to \pi^+\pi^-\pi^0$ and $e^+e^- \to \pi^+\pi^-\pi^0\pi^0$ cross sections are also planned, as are measurements of the inclusive $e^+e^- \to$ *hadrons* cross section in the 2-3 GeV range. The latter results are expected to improve the precision of current 2-3 GeV measurements by about a factor of 2.

The CMD3 experiment at the VEPP-2000 accelerator has also presented preliminary results on the $e^+e^- \to \pi^+\pi^-$ cross section, shown in Fig. 4 (left). The goal is to measure the contribution of the $\pi^+\pi^-$ channel to $a_\mu^{had,LO-VP}$ with a precision of around 0.35%, about half the uncertainty quoted by Babar and KLOE. Final results are expected within a few years. Similarly, the SND experiment at VEPP-2000 has presented preliminary cross section results for $e^+e^- \to \pi^+\pi^-\pi^0$, which are shown in Fig. 4 (right). The CMD3 and SND experiments have, in addition, preliminary results for many other exclusive hadronic channels, such as $e^+e^- \to 2(\pi^+\pi^-\pi^0)$ and the previously unmeasured $e^+e^- \to \pi^+\pi^-\pi^0\eta$ channel, which, when finalized, will lead to substantial improvements in the determination of $a_\mu^{had,LO-VP}$.

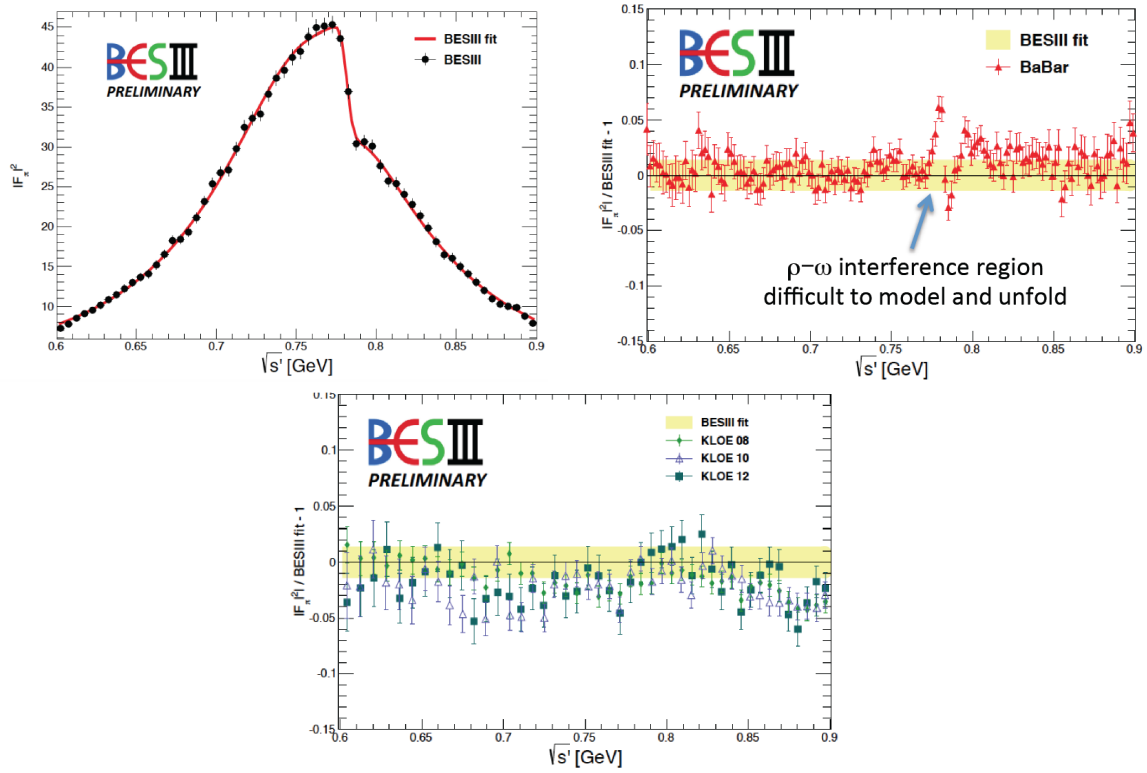

Figure 3: A preliminary BESIII measurement of the $e^+e^- \to \pi^+\pi^-$ cross section is shown in the left plot, along with the result of a fit. The ratio of the Babar and KLOE data with the results of the fit are shown in the center and right plots, respectively.

3. $e^+e^- \to K^+K^-$ from Babar

The discussion will now turn to the Babar program to measure low-energy $e^+e^- \to$ *hadrons* cross sections using the ISR method, which is a long-term project now nearing completion.

Babar recently completed a measurement of the $e^+e^- \to K^+K^-$ cross section and charged kaon form factor [11]. Candidate signal events are required to have exactly two charged tracks with opposite sign that are identified as kaons, each with momentum $p > 1$ GeV. This is a tagged ISR photon analysis, providing high statistical precision at low $\sqrt{s'}$ as needed for the prediction of the muon anomaly. In this and all the Babar tagged ISR studies, the ISR photon is taken to be the highest energy photon in the event, and is required to have an energy in the e^+e^- center-of-mass frame larger than 3 GeV. For this analysis, the ISR photon must lie within 0.3 radians of the missing momentum formed from all the other selected particles in the event, which leads to a strong suppression of non-ISR background events. The remaining background, mostly from other ISR processes such as $\pi^+\pi^-\gamma$, $\mu^+\mu^-\gamma$, and $\pi^+\pi^-\pi^0$ events, is subtracted using data-corrected simulation.

The results for the charged kaon form factor are shown in Fig. 5 (left). Compared with other experiments, Babar covers a larger energy range and generally has more precise results. The result obtained for the K^+K^- contribution to the muon anomaly, $a_\mu^{K^+K^-,LO-VP} = 229.3 \pm 2.8 \times 10^{-11}$, has a precision of 1.2%, compared to a precision of only 3.3% for the previous world average.

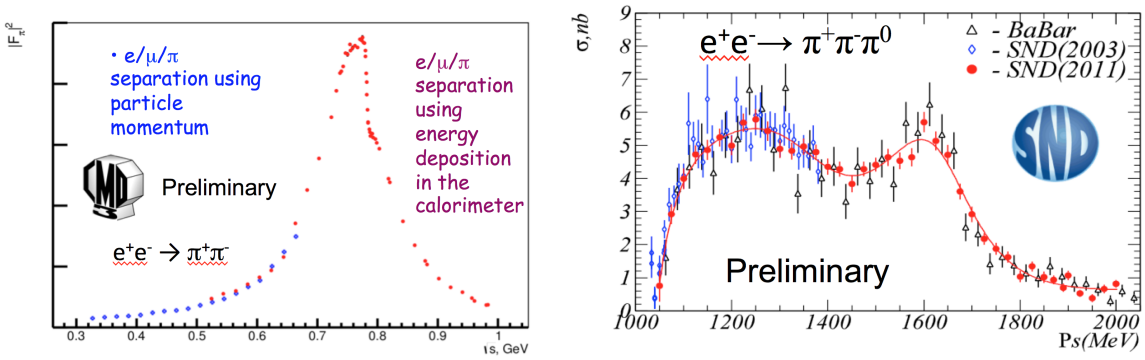

Figure 4: Preliminary results from the (left) CMD3 experiment for the $e^+e^- \to \pi^+\pi^-$ cross section, and (right) SND experiment for the $e^+e^- \to \pi^+\pi^-\pi^0$ cross section.

Figure 5 (left) includes the asymptotic leading-order QCD prediction. The measured form factor is about a factor of four above this prediction, indicating the need to test the theory at higher energies, closer to the asymptotic regime. Above 3 GeV, the statistical precision is greatly improved by using untagged ISR events. Untagged events allow better access to higher $\sqrt{s'} = m_{KK}$ values, better satisfying the asymptotic condition $m_{KK} \to \infty$.

Babar has preliminary results [12] on the charged kaon form factor using untagged ISR $e^+e^- \to K^+K^-$ events. As in the tagged analysis, events are required to contain exactly two charged tracks, with opposite charge, each identified as a kaon. To select events consistent with an undetected ISR photon, viz., one that propagates along the beam direction, the transverse momentum $p_{T,KK}$ of the dikaon system is required to satisfy $p_{T,KK} < 0.15$ GeV, and the missing-mass-squared $|M^2_{miss}| = |(p_{e^+} + p_{e^-} - p_{KK})^2|$ (where "p" indicates a 4-momentum) is required to satisfy $|M^2_{miss}| < 1.0$ GeV. For signal events, the distributions of $p_{T,KK}$ and M^2_{miss} are peaked at zero.

Figure 5 (center) shows the charged kaon form factor results from the untagged K^+K^- analysis ("SA", or small angle) in comparison with the Babar tagged K^+K^- measurements discussed above ("LA", or large angle), and with other results. The greater precision at the higher energy values obtained with the SA study is apparent. The SA results are shown in Fig. 5 (right) in comparison with QCD predictions. At the higher energy scales probed in the SA analysis, the QCD prediction is seen to be in much better agreement with the data than at lower energies, especially when next-to-leading order (NLO) corrections are considered and if the Chernyak and Zhitnitsky (CZ) distribution amplitudes [13] are used.

4. $e^+e^- \to K_SK_L$, $K_SK_L\pi^+\pi^-$, $K_SK_S\pi^+\pi^-$, and $K_SK_SK^+K^-$ from Babar

Babar also has recent results on the $e^+e^- \to K_SK_L$ [14] dikaon cross section, The analysis is based on tagged ISR events. The events are required to contain exactly two charged tracks consistent with a $K_S \to \pi^+\pi^-$ decay and no charged tracks consistent with emanating from the e^+e^- interaction point. The K_L detection efficiency is measured from data using events in the dominant $e^+e^- \to \phi \to K_SK_L$ channel. A very clean K_L signal is observed in the recoil-mass distribution against the $K_S\gamma_{ISR}$ system. Criteria to explicitly identify the K_L are then applied: a cluster with energy $E > 0.2$ GeV in the electromagnetic calorimeter (ECAL) must match the expected K_L di-

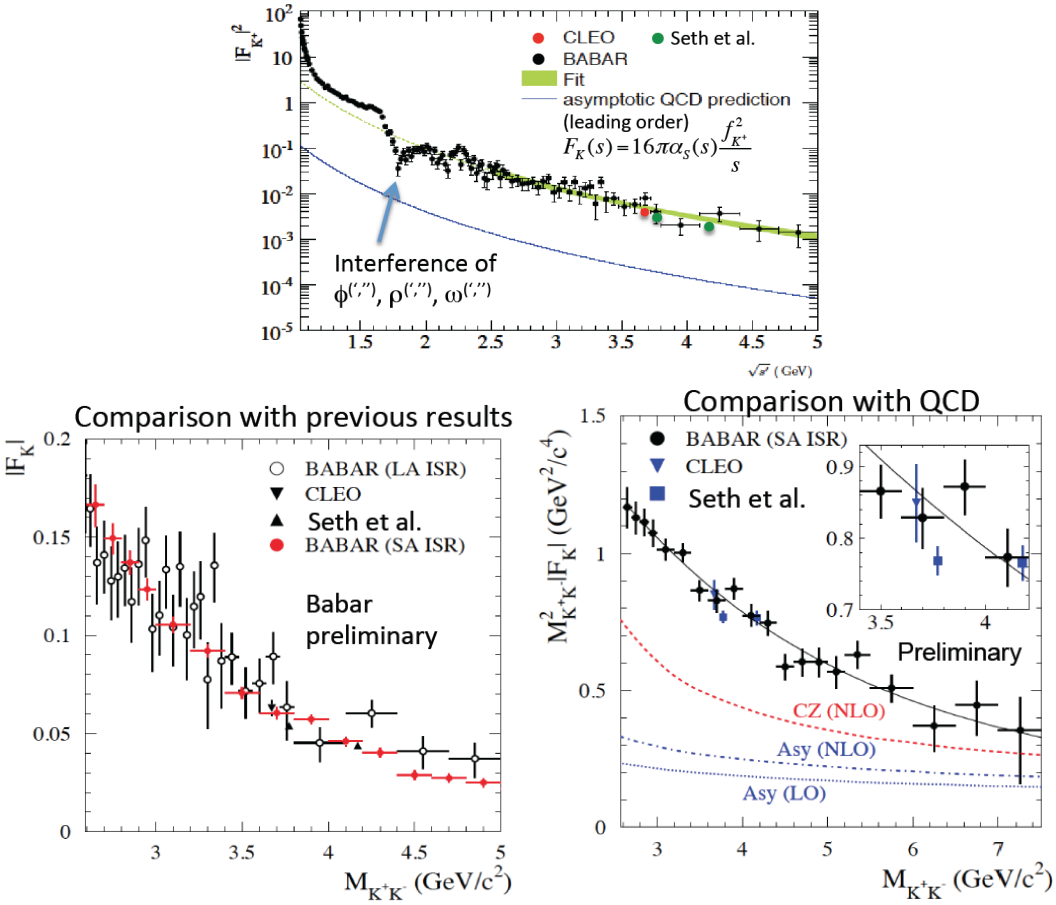

Figure 5: Babar results for the charged kaon form factor, based on (left) tagged ISR photon events and (right and center) untagged ISR photon events.

rection within 0.5 radians. With these criteria, the K_L detection efficiency is found to be 48%, around 2% lower than in simulation. The K_L efficiency is determined as a function of the K_L energy and direction.

The $e^+e^- \to K_S K_L$ cross section in the vicinity of the ϕ meson is shown in Fig. 6 (left). We measure the cross section at energies above the ϕ mass using the observed K_L detection efficiencies. Contributions from $e^+e^- \to K_S K_L(n\pi^0)$ events with $n \geq 1$ are suppressed by requiring the energy of additional ECAL clusters in the event to be less than 0.5 GeV. Data sidebands are used to subtract residual background. The results for the $e^+e^- \to K_S K_L$ cross section above the ϕ are shown in Fig. 6 (center). Clear evidence for resonant structure is seen around 1.6 GeV, possibly due to contributions from the $\omega(1420)$, $\omega(1650)$, $\phi(1680)$, or other mesons. Around 1000 events are found in the region around 1.6 GeV, compared to only 58 events for the only other measurements in this region, from the DM1 experiment [15].

Similar techniques are used to obtain the first measurements of the $e^+e^- \to K_S K_L \pi^+\pi^-$, $K_S K_S \pi^+\pi^-$, and $K_S K_S K^+ K^-$ cross sections. As an example, the results for the $e^+e^- \to K_S K_L \pi^+\pi^-$ cross section are shown in Fig. 6 (right). A clear J/ψ peak is seen. We obtain the first measurements of the J/ψ branching fractions to $K_S K_L \pi^+\pi^-$, $K_S K_S \pi^+\pi^-$, and $K_S K_S K^+ K^-$.

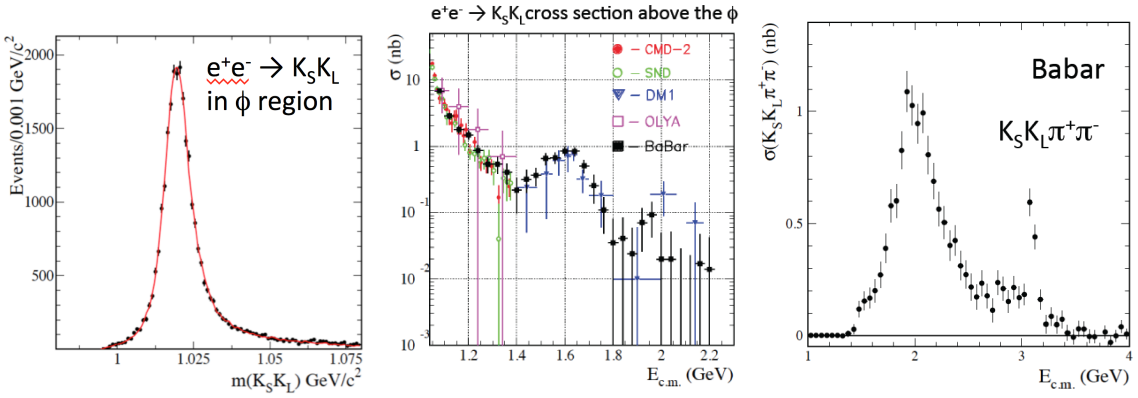

Figure 6: Babar results for the $e^+e^- \to K_SK_L$ cross section (left) in the vicinity of the ϕ meson and (center) above the ϕ, and for the (right) $e^+e^- \to K_SK_L\pi^+\pi^-$ cross section

5. $e^+e^- \to K_SK^+\pi^-\pi^0$ and $K_SK^+\pi^-\eta$ from Babar

A final topic is the first measurement of the $e^+e^- \to K_SK^+\pi^-\pi^0$ and $K_SK^+\pi^-\eta$ cross sections. These results, based on tagged ISR events from Babar, are preliminary. The analysis requires at least one $K_S \to \pi^+\pi^-$ candidate consistent with the interaction point, two photons with a diphoton invariant mass consistent either with a π^0 or η meson, and two oppositely charged tracks, one identified as a pion and one as a kaon. Background from the non-ISR processes $e^+e^- \to K_SK^+\pi^-\pi^0\pi^0$ and $K_SK^+\pi^-\eta\pi^0$ is evaluated from simulation, with the normalization for the simulated curves adjusted to fit the reconstructed $\pi^0 \to \gamma\gamma$ peak in data. Background from the ISR processes $e^+e^- \to K_SK^+\pi^-$, $K_SK^+\pi^-\pi^0\pi^0$, and $K_SK^+\pi^-\eta\pi^0$ (either one more or one less π^0 than signal events) is evaluated from data sidebands.

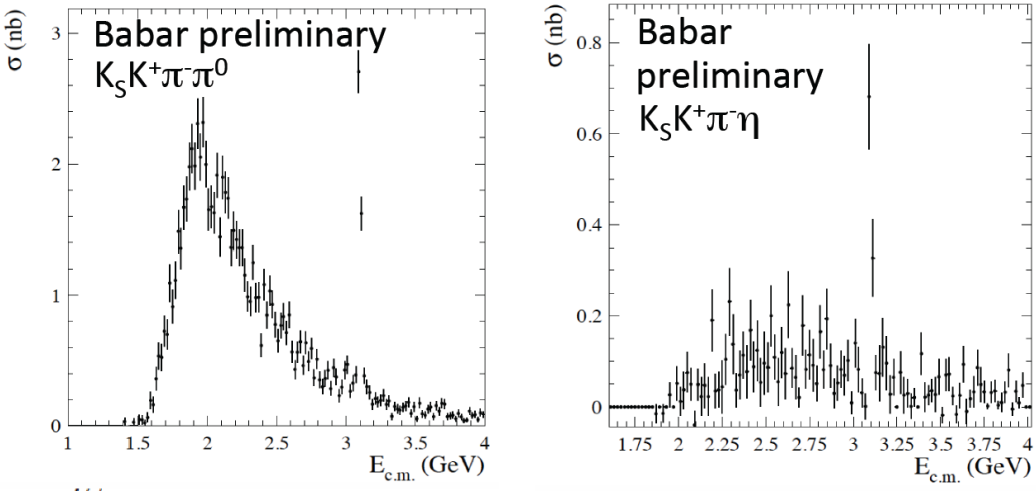

Figure 7: Babar results for the (left) $e^+e^- \to K_SK^+\pi^-\pi^0$ and (right) $e^+e^- \to K_SK^+\pi^-\eta$ cross sections.

The results for the cross sections are shown in Fig. 7. As for the neutral dikaon channels discussed in Section 4, clear J/ψ peaks are seen. We obtain the first measurement of the J/ψ

branching fraction to $K_S K^+ \pi^- \pi^0$. For $J/\psi \to K_S K^+ \pi^- \eta$, one previous measurement exists [16]: the preliminary Babar result lies around 2 standard deviations below this previous result.

6. Conclusion

In summary, precise low-energy measurements of e^+e^- hadronic cross sections are needed to obtain an accurate standard model prediction for the leading-order hadronic vacuum polarization term $a_\mu^{had,LO-VP}$ of the muon anomalous magnetic moment. The Babar and KLOE results for the $e^+e^- \to \pi^+\pi^-$ cross section – the most important measurement for $a_\mu^{had,LO-VP}$ – are not consistent with each other. New, precise results on $e^+e^- \to \pi^+\pi^-$ are expected from BESIII, CMD, and SND, which will hopefully resolve this discrepancy. In addition, precise new results on $e^+e^- \to \pi^+\pi^-\pi^0$ and $e^+e^- \to \pi^+\pi^-\pi^0\pi^0$ are expected to be forthcoming. With the new data, it is estimated that the uncertainty in $a_\mu^{had,LO-VP}$ might be reduced by around a factor of 2 [17].

The Babar program to measure low-energy e^+e^- hadronic cross sections, based on the initial-state photon radiation method, has produced many precise results and is now almost complete. The Babar results presented here emphasize recent results with charged and neutral kaons in the final state, which provide new information, tests of QCD, and first observations of cross sections and J/ψ branching fractions.

The author would like to thank Achim Denig and Sergey Serednyakov for providing information respectively about the BES and SND/CMD3 programs.

References

[1] F. Jegerlehner and A. Nyffeler, Phys. Rept. **477** (2009) 1.

[2] T. Aoyama, M. Hayakawa, T, Kinoshita, and M. Nio, Phys. Rev. Lett. **109** (2012) 111808.

[3] C. Gnendiger, D. Stöckinger, and H. Stöckinger-Kim, Phys. Rev. D **88** (2013) 053005.

[4] M. Davier, A. Hoecker, B, Malaescu, and Z. Zhang, Z. Phys. C **71** (2011) 1515.

[5] G. W. Bennett et al. (E821 Collaboration), Phys. Rev. D **73** (2006) 072003.

[6] K. A. Olive et al. (Particle Data Group), Chin. Phys. C **38** (2014) 090001.

[7] M. Della Morte, B. Jäger, A. Jüttner, and H. Wittig, JHEP **03** (2012) 055.

[8] J. P. Lees et al. (Babar Collaboration), Phys. Rev. D **86** (2012) 032013.

[9] F. Ambrosino et al. (KLOE Collaboration), Phys. Lett. B **700** (2011) 102.

[10] D. Babusci et al. (KLOE Collaboration). Phys. Lett. B **720** (2013) 336.

[11] J. P. Lees et al. (Babar Collaboration), Phys. Rev. D **88** (2013) 032013.

[12] J. P. Lees et al. (Babar Collaboration), arXiv:1507.04638, submitted to Phys. Rev. D.

[13] V. L. Chernyak and A. R. Zhitnitsky, Phys. Rept. **112** (1984) 173.

[14] J. P. Lees et al. (Babar Collaboration), Phys. Rev. D **89** (2014) 092002.

[15] F. Manè et al. (DM1 Collaboration), Phys. Lett. B **99** (1981) 261.

[16] M. Ablikim et al. (BES Collaboration), Phys. Rev. D **77** (2008) 032005.

[17] T. Blum et al., arXiv:1311.2198 (2013).